ACS APPLIED POLYMER MATERIALS

pubs.acs.org/acsapm Article

Substituted Thioxanthone-Based Photoinitiators for Efficient Two-Photon Direct Laser Writing Polymerization with Two-Color Resolution

Teng Chi, Paul Somers, Daniel A. Wilcox, Ashley J. Schuman, Jason E. Johnson, Zihao Liang, Liang Pan, Xianfan Xu, and Bryan W. Boudouris*

Cite This: https://dx.doi.org/10.1021/acsapm.0c01291 Read Online

ACCESS | Metrics & More | Article Recommendations | Supporting Information

ABSTRACT: Nanolithographic printing by direct laser writing (DLW) photopolymerization has attracted increased attention in recent years, as the speed of this printing has increased, while the feature sizes that have been realized have decreased well into the nanoscale regime. Specifically, isopropyl thioxanthone (ITX) has been utilized as one of the common photoinitiators in DLW polymerization processes because of its high-efficiency photoinitiating abilities and its ability to have its initiation properties inhibited through the application of a second wavelength of light. However, improved photoinitiating materials that are built from this successful archetype are required, by both academic and industrial circles, if advanced high-throughput nanomanufacturing techniques are to be implemented. Here, next-generation thioxanthone-based photoinitiators with tailored optical and charge transfer properties were computationally designed and subsequently synthesized. Particularly, branches with specifically modulated electron donor and electron acceptor qualities, relative to the ITX core, were coupled to the initial thioxanthone substrate. After having their molecular and optical properties characterized in full, it was evident that these initiators possessed a clear advancement in terms of photopolymerization initiation relative to ITX. As such, a champion photoinitiator chemistry was brought forward to demonstrate enhanced two-photon polymerization DLW such that superresolution properties were exhibited. In this way, we introduce a clear means by which to systematically design future photoinitiators for enhanced two-photon polymerization DLW nanoprinting processes.

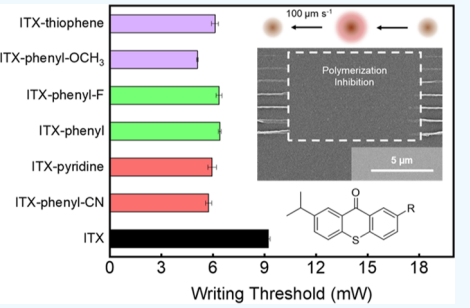

KEYWORDS: *thioxanthone-based photoinitiators, two-photon polymerization nanoprinting, direct laser writing, high-speed nanolithography, low-temperature phosphorescence spectroscopy*

Downloaded via PURDUE UNIV on February 26, 2021 at 23:04:49 (UTC).
See https://pubs.acs.org/sharingguidelines for options on how to legitimately share published articles.

INTRODUCTION

Direct laser writing (DLW) has developed rapidly in recent years, and it has become an essential process for three-dimensional (3D) nanofabrication. Specifically, the two-photon polymerization (2PP) DLW process has found use in a diverse range of fields including nanophotonics,[1−3] microrobotics,[4−6] microfluidics,[7−9] metamaterials,[10−12] micro-optics,[13] security,[14] and bioengineering.[15−17] The high spatial resolution associated with the 2PP process provides an advantage relative to other nanofabrication techniques. Unlike single-photon absorption, two-photon absorption is confined to the focal region of a tightly focused laser beam, which occurs because of nonlinear, multiphoton absorption. This gives rise to the submicron 3D structuring capabilities now expected of 2PP-DLW. Unfortunately, the two-photon absorption process is typically not efficient, resulting in relatively large laser power requirements. While the current power requirements are suitable for single-beam 2PP-DLW processes, power becomes an issue when attempting to scale production with multiple beams or image projection. In turn, this has prompted the development of photoinitiator molecules with superior absorption abilities in the polymerization reaction medium.[21] Recent efforts have resulted in significant steps toward designing photoinitiating molecules with dramatically improved two-photon photoinitiation performance.[18−20] In one case, it was shown that combining general design guidelines with proper laser wavelength choice leads to near-resonance enhancement of the two-photon absorption properties in the photoinitiator and a laser power requirement eight times lower than commercial initiators.[19] Beyond only power requirements, in many instances, the current achievable spatial resolution of 2PP is not to the point where it is of utility in all operations, and this necessitates the use of resolution-enhancing strategies

Received: November 19, 2020
Accepted: February 7, 2021

© XXXX American Chemical Society

for 2PP-DLW.[21] By introducing a secondary laser into the DLW system, precise spatial control of the polymerization region can be achieved via a polymerization inhibition process. This leads to significantly increased DLW resolution (i.e., super resolution), with resolution limits on the order of 120 nm being achieved.[22] Inhibition of the polymerization process via a secondary laser is reliant on the properties of the photoinitiator used. Currently, only a limited number of photoinitiators are known to achieve this polymerization inhibiting effect for controlling the 2PP-DLW process, and the library of photoinitiator candidates needs to be expanded significantly, such that this promising nanotechnology application space can reach its full potential.

The choice of the 2PP-DLW photoinitiator can depend on the desired polymerization initiation pathway. Generally, photoinitiators are housed within two classes.[23,24] Norrish Type I initiators are molecules that generate radicals directly by photocleavage. Norrish Type II initiators absorb light to form excited states that abstract hydrogen from a coinitiator to generate radicals. In DLW, the widely used, commercially available photoinitiator 2-isopropylthioxanthone (ITX) is a special Type II initiator that operates intramolecularly without the use of a coinitiator. Modification of the ITX photoinitiator for superior absorption properties has been the base of many promising and informative efforts for photoinitiator design strategies.[25−30] During the design of 2PP photoinitiators, it has been observed that molecules that follow a donor−acceptor−donor structure present themselves as stronger two-photon initiators.[31] Holding to this idea, molecular branches attached to the ITX core have been synthesized previously, and this led to improved photoinitiating properties.[27,32] However, several of the synthesized molecules suffered from low synthesis yield, poor solubility, and poor stability.[32] Along with the wealth of knowledge available for modifying this fairly well-known initiator, ITX is especially of interest here as its photoinitiation ability can be turned off through exposure to a secondary laser during the DLW polymerization process, which results in extremely high-resolution nanoprinting.[21,33,34] Thus, this is a promising molecule to derivatize to further enhance the polymerization initiation and inhibition properties that could lead to superior 2PP-DLW performance.

In this work, the abovementioned barriers were overcome through an improved molecular design motif. That is, the newly designed photoinitiators continue to achieve superior absorption properties compared to ITX, while having high synthetic yields, good solubility in a common monomer resin, and long-term ambient stability. For these photoinitiators, the isopropyl group common to ITX was maintained, and this allowed the molecules to be readily soluble in the monomer. To provide a guideline for the synthesis routes, the absorption spectra of the new photoinitiators were obtained using time-dependent density functional theory (TD-DFT). The possibility of charge transfer states was predicted by measuring the frontier molecular orbitals of the photoinitiating molecules. The two-photon cross sections of each of the synthesized photoinitiators were measured using the *Z*-scan technique to provide an indicator of two-photon absorption efficiency in DLW. Phosphorescence spectra were used to obtain triplet excited-state lifetimes, as the triplet state is vital in initiating the polymerization reaction and the polymerization inhibition process with these photoinitiators. Finally, the polymerization initiation efficiency of the photoinitiators was determined via 2PP-DLW. In addition, the polymerization inhibition capability during 2PP-DLW was established. By determining the properties of these new photoinitiators and performing nanolithographic printing, we demonstrate a practical pathway to achieve low-power and high-resolution 3D photopolymerization through advanced photoinitiator design.

MATERIALS AND GENERAL EXPERIMENTAL PROCEDURES

Phenylboronic acid pinacol ester, 4-methoxyphenylboronic acid pinacol ester, 4-cyanophenylboronic acid pinacol ester, and 4-fluorophenylboronic acid pinacol ester were purchased from Oakwood. All other chemicals were purchased from Sigma-Aldrich, and all chemicals were used as received. All ultraviolet−visible (UV−vis) light spectroscopy data were obtained using a Cary 60 spectrometer in the wavelength range of $330 \leq \lambda \leq 800$ nm. Fluorescence and phosphorescence spectroscopy data were collected on a Cary Eclipse fluorescence and phosphorescence spectrophotometer in the wavelength range of 400 nm $\leq \lambda \leq$ 800 nm. Phosphorescence data were collected at $T = 77$ K using deoxygenated solutions of the samples in a glass-forming solvent, toluene. For these measurements, the optical absorbance was below 0.01 at the excitation wavelength. Finally, the computational results were performed as described previously.[32]

Synthesis of 2-Bromo-7-isopropyl-9*H*-thioxanthen-9-one (ITX-Br, Compound 1). 2-Isopropyl-9*H*-thioxanthen-9-one (6.4 g, 25 mmol) was added to a 250 mL round bottom flask with 50 mL of dichloromethane. Then, zinc chloride (0.35 g, 2.5 mmol) was poured, while the reaction mixture was held at 0 °C. After the addition of zinc chloride, bromine (8 g, 50 mmol) in 50 mL of dichloromethane was added in a dropwise manner. Then, the temperature was gradually increased to 25 °C. After 24 h, a dark red solution formed, and the solution was quenched by $NaHSO_3$ and extracted with dichloromethane and water three times. After evaporation of the organic solvent, a light-yellow solid was dissolved into toluene and subsequently recrystallized to form white crystals in 65% yield. ^{1}H NMR (400 MHz, chloroform-*d*): δ 8.75 (dd, J = 2.3, 0.4 Hz, 1H), 8.48 (d, J = 1.9 Hz, 1H), 7.70 (dd, J = 8.6, 2.3 Hz, 1H), 7.53 (dd, J = 3.5, 1.3 Hz, 2H), 7.46 (dd, J = 8.6, 0.4 Hz, 1H), 3.07 (p, J = 6.9 Hz, 1H), 1.33 (d, J = 6.9 Hz, 6H).

Synthesis of 2-Isopropyl-7-(pyridin-4-yl)-9*H*-thioxanthen-9-one (ITX-Pyridine, Compound 2). 2-Bromo-7-isopropyl-9*H*-thioxanthen-9-one (ITX-Br, 66 mg, 0.2 mmol) was added to a 10 mL sealed tube with 1 mL of toluene. Then, 4-(4,4,5,5-tetramethyl-1,3,2-dioxaborolan-2-yl)pyridine (45 mg, 0.22 mmol) and 0.5 mL of 1 M Na_2CO_3 in water were added. Next, tetrakis(triphenylphosphine) palladium(0) (12 mg, 0.01 mmol) was added with 0.5 mL of ethanol. The reaction turned red. After three freeze−pump−thaw cycles, the sealed tube was slowly heated to 90 °C. After 24 h, the organic mixture was washed with brine three times and deionized (DI) water three times, followed by extraction with ethyl acetate. The mixture was purified by column chromatography (Hexane/ethyl acetate = 3:1 v/v) to yield a solid with 83% yield. ^{1}H NMR (400 MHz, chloroform-*d*): δ 8.93 (d, J = 2.1 Hz, 1H), 8.76−8.68 (m, 2H), 8.51 (s, 1H), 7.89 (dd, J = 8.4, 2.1 Hz, 1H), 7.71 (d, J = 8.4 Hz, 1H), 7.67−7.61 (m, 2H), 7.56 (d, J = 1.5 Hz, 2H), 3.09 (p, J = 6.9 Hz, 1H), 1.34 (d, J = 6.9 Hz, 6H).

Synthesis of 4-(7-Isopropyl-9-oxo-9*H*-thioxanthen-2-yl)-benzonitrile (ITX-Phenyl-CN, Compound 3). 2-Bromo-7-isopropyl-9*H*-thioxanthen-9-one (ITX-Br, 66 mg, 0.2 mmol) was added to a 10 mL sealed tube with 1 mL of toluene. Then, 4-(4,4,5,5-tetramethyl-1,3,2-dioxaborolan-2-yl)benzonitrile (51 mg, 0.22 mmol) was added. After this addition, 0.5 mL of 1 M Na_2CO_3 in water was added. Tetrakis(triphenylphosphine)palladium(0) (12 mg, 0.01 mmol) was added with 0.5 mL of ethanol. The reaction turned red. After three freeze−pump−thaw cycles, the sealed tube was slowly heated to 90 °C. After 24 h, the crude mixture was obtained; the organic solution was washed with brine three times and DI water three times, followed by extraction with ethyl acetate. The extracted organic layer was purified by column chromatography after evaporation of ethyl acetate (Hexane/ethyl acetate = 20:1 v/v) to

https://dx.doi.org/10.1021/acsapm.0c01291
ACS Appl. Polym. Mater. XXXX, XXX, XXX−XXX

yield a solid with 90% yield. ^{1}H NMR (800 MHz, chloroform-*d*): δ 8.89 (d, J = 2.2 Hz, 1H), 8.53 (d, J = 1.9 Hz, 1H), 7.88−7.85 (m, 1H), 7.85−7.82 (m, 2H), 7.81−7.78 (m, 2H), 7.72 (d, J = 8.2 Hz, 1H), 7.60−7.57 (m, 2H), 3.11 (p, J = 7.0 Hz, 1H), 1.36 (d, J = 7.0 Hz, 6H).

Synthesis of 2-Isopropyl-7-phenyl-9*H*-thioxanthen-9-one (ITX-Phenyl, Compound 4). 2-Bromo-7-isopropyl-9*H*-thioxanthen-9-one (ITX-Br, 66 mg, 0.2 mmol) was added to a 10 mL sealed tube with 1 mL of toluene. Then, 4,4,5,5-tetramethyl-2-phenyl-1,3,2-dioxaborolane (45 mg, 0.22 mmol) and 0.5 mL of 1 M Na_2CO_3 in water were added. After the addition of the Na_2CO_3 solution, tetrakis(triphenylphosphine) palladium(0) (12 mg, 0.01 mmol) was added with 0.5 mL of ethanol. The reaction turned an orangish-red color. After three freeze−pump−thaw cycles, the sealed tube was slowly heated to 90 °C. After 24 h, the crude mixture was obtained; the organic solution was washed with brine three times and extracted with ethyl acetate. The mixture was purified by column chromatography after evaporation of ethyl acetate (Hexane/ethyl acetate = 16:1 v/v) to yield a solid with 80% yield. ^{1}H NMR (400 MHz, chloroform-*d*): δ 8.88 (d, J = 2.2 Hz, 1H), 8.52 (s, 1H), 7.87 (dd, J = 8.4, 2.1 Hz, 1H), 7.72 (d, J = 7.2 Hz, 2H), 7.65 (d, J = 8.3 Hz, 1H), 7.54 (d, J = 1.4 Hz, 2H), 7.49 (t, J = 7.7 Hz, 2H), 7.41 (d, J = 7.4 Hz, 1H), 3.08 (p, J = 6.9 Hz, 1H), 1.34 (d, J = 6.9 Hz, 7H).

Synthesis of 2-(4-Fluorophenyl)-7-isopropyl-9*H*-thioxanthen-9-one (ITX-Phenyl-F, Compound 5). 2-Bromo-7-isopropyl-9*H*-thioxanthen-9-one (ITX-Br, 66 mg, 0.2 mmol) was added to a 10 mL sealed tube with 1 mL of toluene. Then, 2-(4-fluorophenyl)-4,4,5,5-tetramethyl-1,3,2-dioxaborolane (49 mg, 0.22 mmol) and 0.5 mL of 1 M Na_2CO_3 in water solution were added. Tetrakis (triphenylphosphine) palladium(0) (12 mg, 0.01 mmol) and 0.5 mL of ethanol were added sequentially, and the reaction turned orange. After three freeze−pump−thaw cycles, the sealed tube was slowly heated to 90 °C. After 24 h, the crude mixture was obtained; the organic solution was washed with brine three times and DI water three times, followed by extraction with ethyl acetate. The mixture was purified by column chromatography after evaporation of ethyl acetate (Hexane/ethyl acetate = 20:1 v/v) to yield a solid with 76% yield. ^{1}H NMR (800 MHz, chloroform-*d*): δ 8.82 (d, J = 2.2 Hz, 1H), 8.53 (s, 1H), 7.82 (dd, J = 8.3, 2.1 Hz, 1H), 7.68 (dd, J = 8.5, 5.5 Hz, 2H), 7.65 (d, J = 8.3 Hz, 1H), 7.55 (d, J = 1.5 Hz, 2H), 7.19 (t, J = 8.6 Hz, 2H), 3.10 (p, J = 7.1 Hz, 1H), 1.36 (d, J = 7.0 Hz, 6H).

Synthesis of 2-Isopropyl-7-(4-methoxyphenyl)-9*H*-thioxanthen-9-one (ITX-Phenyl-OCH$_3$, Compound 6). 2-Bromo-7-isopropyl-9*H*-thioxanthen-9-one (ITX-Br, 66 mg, 0.2 mmol) was added to a 10 mL sealed tube with 1 mL of toluene. Then, 2-(4-methoxyphenyl)-4,4,5,5-tetramethyl-1,3,2-dioxaborolane (52 mg, 0.22 mmol) and 0.5 mL of 1 M Na_2CO_3 in water were added. After the addition of the Na_2CO_3 solution, tetrakis(triphenylphosphine) palladium(0) (12 mg, 0.01 mmol) was added with 0.5 mL of ethanol. After three freeze−pump−thaw cycles, the sealed tube was slowly heated to 90 °C. After 24 h, the crude mixture was obtained; the organic solution was washed with brine three times and DI water three times, followed by extraction with ethyl acetate. The mixture was purified by column chromatography (Hexane/ethyl acetate = 15:1 v/v) to yield a solid with 81% yield. ^{1}H NMR (400 MHz, chloroform-*d*): δ 8.82 (s, 1H), 8.52 (d, J = 0.6 Hz, 1H), 7.80 (dd, J = 8.4, 2.2 Hz, 1H), 7.78−7.68 (m, 1H), 7.66−7.62 (m, 2H), 7.59 (dd, J = 8.4, 0.5 Hz, 1H), 7.50−7.40 (m, 1H), 7.01 (d, J = 8.8 Hz, 2H), 3.86 (s, 3H), 3.07 (pd, J = 6.9, 0.7 Hz, 1H), 1.34 (d, J = 6.9 Hz, 6H).

Synthesis of 2-Isopropyl-7-(thiophen-2-yl)-9*H*-thioxanthen-9-one (ITX-Thiophene, Compound 7). 2-Bromo-7-isopropyl-9*H*-thioxanthen-9-one (ITX-Br, 66 mg, 0.2 mmol) was added to a 10 mL sealed tube with 1 mL of toluene. Then, 4,4,5,5-tetramethyl-2-(thiophen-2-yl)-1,3,2-dioxaborolane (46 mg, 0.22 mmol) and 0.5 mL of 1 M Na_2CO_3 in water were added. After the addition of Na_2CO_3 solution, tetrakis(triphenylphosphine)palladium(0) (12 mg, 0.01 mmol) was added with 0.5 mL of ethanol. The reaction turned red. After three freeze−pump−thaw cycles, the sealed tube was slowly heated to 90 °C. After 24 h, the mixture was washed with brine three times and DI water three times, followed by extraction with ethyl acetate. The mixture was purified by column chromatography (Hexane/ethyl acetate = 10:1 v/v) to yield a solid with 77% yield. 1H NMR (400 MHz, $CDCl_3$): δ 8.88 (d, J = 2.1 Hz, 1H), 8.53 (s, 1H), 7.88 (dd, J = 8.4, 2.2 Hz, 1H), 7.61 (d, J = 8.4 Hz, 1H), 7.56 (d, J = 1.2 Hz, 2H), 7.50 (dd, J = 3.6, 1.1 Hz, 1H), 7.37 (dd, J = 5.1, 1.1 Hz, 1H), 7.15 (dd, J = 5.1, 3.6 Hz, 1H), 3.10 (dd, J = 13.8, 6.9 Hz, 1H), 1.36 (d, J = 6.9 Hz, 6H).

DLW Photopolymerization. DLW was performed using a custom-built fabrication system, and the details of the experimental setup have been reported previously.[32] The printing laser consisted of an 800 nm femtosecond oscillator (Coherent Micra) at an 80 MHz repetition rate. A full width at a half-maximum pulse width of ∼390 fs at the sample plane was determined by autocorrelation measurement. A 100× oil-immersion objective lens (Nikon, N.A. = 1.49) was used to focus the laser beam into the photoresist to induce polymerization. Fabrication was achieved by motion of the sample via a nanopositioner (Mad City Labs) and laser control by a fast mechanical shutter (Uniblitz) that was controlled with a custom LabVIEW code. The laser power was adjusted through combined use of a half-wave plate and a polarizer. Photoresist samples were sandwiched between a microscope slide and a coverslip, and tape was used to provide a ∼35 μm gap between the two pieces of glass. All printing was performed at a rate of 100 μm s^{-1} writing speed. For polymerization inhibition experiments, a 638 nm continuous wave laser was introduced to the beam path by a dichroic beam splitter and controlled independently by a variable neutral density filter and fast shutter (Uniblitz). The 638 nm beam was passed through a telescoping lens pair to achieve a focus spot size significantly larger than that of the 800 nm laser at the sample. The laser powers for both beams were measured at the back of the objective lens through a 6 mm diameter aperture. Fabricated structures were developed in an isopropanol bath for 10 min, rinsed with isopropanol, and dried with nitrogen. Fabricated structures were observed under an optical microscope in transmission mode. The selected samples were sputter-coated with ∼13 nm of an Au/Pd mixture before imaging with a scanning electron microscope (Hitachi S-4800) to prevent charging.

***Z*-Scan Measurements.** Two-photon absorption cross sections were measured using an open aperture *Z*-scan.[35] *Z*-scan measurements were performed using 60 fs pulses at an 800 nm center wavelength from a 5 kHz regeneratively amplified laser (Spectra-Physics Spitfire). Solutions of each photoinitiator in tetrahydrofuran were prepared in a 1 mm path length cuvette for measurement, and these concentrations are listed in Table S1. Each sample was translated along the optical (*z*-) axis by a motorized stage, and the transmitted beam was collected with a balanced photodetector (New Focus 2307). The signal from the photodetector was passed through a lock-in amplifier referencing the laser repetition rate. A Rayleigh range for the laser of 3 mm was fit from the measured data. Transmission values of the samples were fit using eq 1.[35]

$$T(z) = \sum_{m=0}^{\infty} \frac{[-q_0(z, 0)]^m}{(m+1)^{3/2}} \tag{1}$$

where

$$q_0(z, t) = \frac{\beta I_0(t) L_{\text{eff}}}{\left(1 + \frac{z^2}{z_0^2}\right)} \tag{2}$$

Here, β is the two-photon absorption coefficient, $I_0(t)$ is the peak intensity at the focus of the beam, L_{eff} is the effective thickness of the sample (taken to be the cuvette path length), and z_0 is the Rayleigh length of the beam. The sample position (z) is measured relative to the minimum beam waist location. The two-photon cross section was determined according to eq 3.

$$\sigma_2 = \frac{\beta E_{\text{photon}}}{\rho_{\text{mol}}} \tag{3}$$

Here, E_{photon} is the photon energy of 800 nm photon and ρ_{mol} is the density of the photoinitiator molecules in the solution.

https://dx.doi.org/10.1021/acsapm.0c01291
ACS Appl. Polym. Mater. XXXX, XXX, XXX−XXX

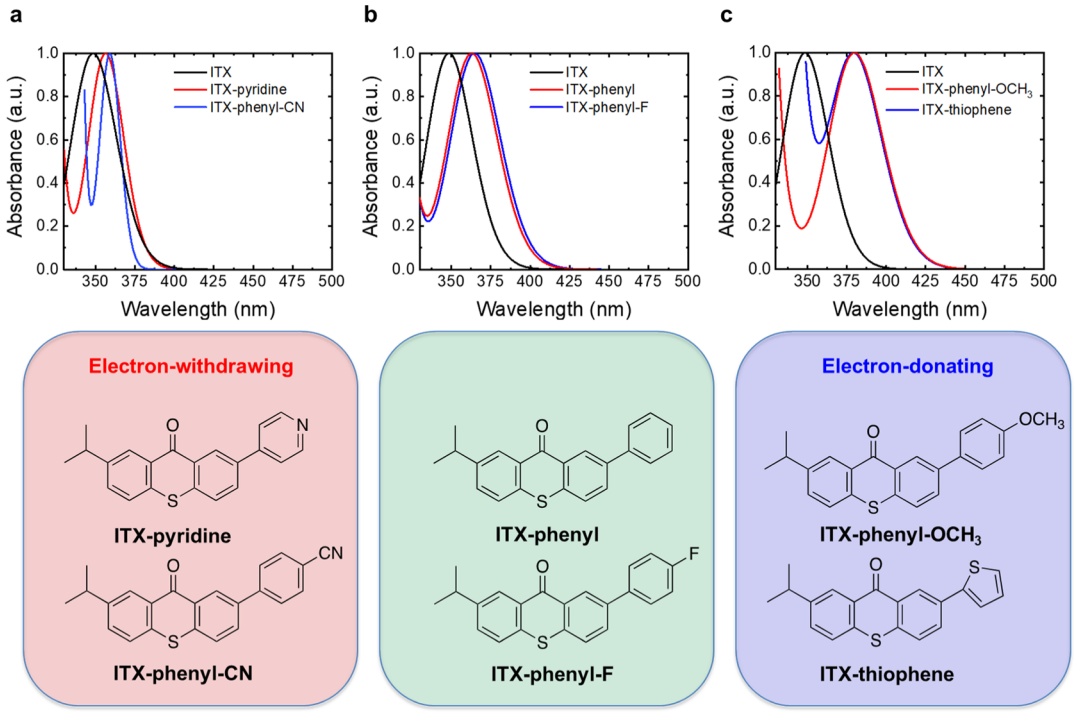

Figure 1. Predicted UV−Vis light absorption plots for: (a) ITX, ITX-pyridine, and ITX-phenyl-CN; (b) ITX, ITX-phenyl, and ITX-phenyl-F; and (c) ITX, ITX-phenyl-OCH_3, and ITX-thiophene. These predictions were made using TD-DFT with a B3LYP/6-31G(d) level of theory. The structures of the calculated initiating molecules (aside from ITX) are listed directly below their simulated absorption spectra.

RESULTS AND DISCUSSION

According to previous efforts,[36] ITX and its derivatives have the potential to be high-performance radical initiating photoinitiators in the 2PP-DLW processes. Here, we build from this previous work to modify the photoinitiator molecular design in a strategic manner. Specifically, new branches to the ITX core were introduced and classified into three groups based on their chemical construct. Specifically, these were substituents that were (1) electron-withdrawing groups, including 7-isopropyl-2-(pyridin-4-yl)-4*aH*-thioxanthen-9-(9*aH*)-one (ITX-pyridine) and 4-(7-isopropyl-9-oxo-9,9*a*-dihydro-4*aH*-thioxanthen-2-yl)benzonitrile (ITX-phenyl-CN); (2) electron-donating groups, including 7-isopropyl-2-(4-methoxyphenyl)-4*aH*-thioxanthen-9(9*aH*)-one (ITX-phenyl-OCH_3) and 7-isopropyl-2-(thiophen-2-yl)-4*aH*-thioxanthen-9(9*aH*)-one (ITX-thiophene); and (3) groups that were neither strongly electron-accepting nor electron-donating, namely, 7-isopropyl-2-phenyl-4*aH*-thioxanthen-9(9*aH*)-one (ITX-phenyl) and 2-(4-fluorophenyl)-7-isopropyl-4*aH*-thioxanthen-9(9*aH*)-one (ITX-phenyl-F). In all cases, the additional chemical functionality is added in a manner that makes the substituents conjugated with the core ITX structure. The molecules' branch designs follow the donor−acceptor type structures popularly suggested for two-photon initiators.

To guide this molecular design, TD-DFT calculations were utilized to predict the absorption spectra of these proposed initiators (Figure 1).[37] This computational design could be implemented in a straightforward manner here, as all relevant optical transitions for similar molecules have been established previously.[32] The computational predictions indicated that the proposed molecules should have an absorption peak that is red-shifted relative to ITX. This is expected to increase the laser writing efficiency of the 800 nm 2PP-DLW, as increasing absorption at a wavelength of 400 nm is key to an efficient photoinitiation process. Moreover, these three groups reveal a trend with respect to the optical absorption characteristics and how this design motif can be utilized to tune the absorption profile. Specifically, the ITX-based molecules with electron-donating groups showed the greatest redshift, while ITX-based molecules with electron-withdrawing groups present in the structure showed the least amount of the absorption shift. Inspired by the TD-DFT calculation results, these molecules based on an ITX core with different substituent groups were synthesized to experimentally verify their potential as photoinitiating candidates and to support or refute this predicted trend.

Six different substituents were altered in a systematic way, as functionalization of the conjugated branch afforded a means by which to evaluate multiple distinct chemical functionalities while maintaining a common chemical core for the photoinitiators. These added functionalities extend aromaticity across the molecular systems, which changed the optical properties dramatically. A straightforward synthetic pathway was utilized to create the new photoinitiators (Scheme 1), and these compounds were characterized by ^{1}H NMR spectroscopy and ^{13}C NMR spectroscopy (Figures S1−S6). Specifically, 2-bromo-7-isopropyl-9*H*-thioxanthen-9-one (ITX-Br) was synthesized from ITX using a bromination reaction catalyzed by zinc chloride.[38−41] Then, the six different substituents were introduced through Suzuki coupling reactions.[42−47] The final molecular targets are air-stable and insensitive to ambient conditions.

An improved excited state lifetime is predicted for the modified ITX molecules as the result of a direct highest occupied molecular orbital (HOMO) to lowest unoccupied molecular orbital (LUMO) transition. The frontier molecular orbitals were calculated and are shown in Figure S7. The thioxanthone core can be regarded as an acceptor and the

https://dx.doi.org/10.1021/acsapm.0c01291
ACS Appl. Polym. Mater. XXXX, XXX, XXX−XXX

Scheme 1. Synthetic Pathway for the New ITX-Based Photoinitiators

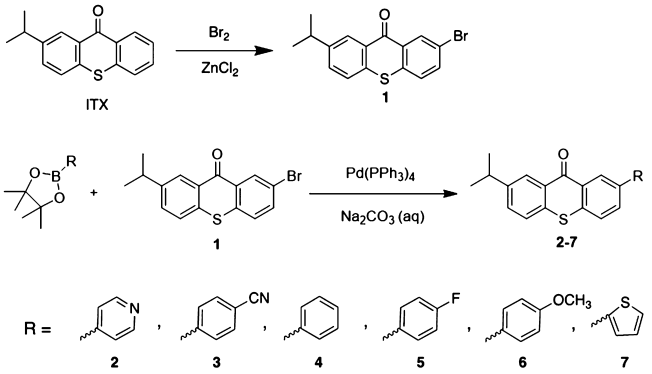

introduced branch as the donor. The lowest-energy singlet excited state for each of the initiator candidates is a transition from the HOMO to the LUMO. This is a significant contrast from the photoinitiators we described previously.[32] That is, while the lowest-energy singlet excited state was a HOMO to LUMO transition in this previous effort, it was an optically inactive charge-transfer state, with the first optically active state involving both HOMO − 1 to LUMO and HOMO to LUMO + 1 transitions. Importantly, this means that the excited states associated with the molecules of the current effort should have fewer alternative pathways beyond that required for polymerization because no lower singlet excited states by which to decay were available.

To evaluate these computational predictions, the optical properties of the new initiators were measured and compared with the computational results. First, the molar absorption coefficients of the photoinitiators at half the wavelength (400 nm) of 2PP-DLW (800 nm) were measured in toluene (Table 1), and the normalized UV−vis absorption spectra were plotted (Figure S8a). Although there is a difference between the one-photon absorption process in this test and the two-photon absorption process that occurs in the DLW process,[48,49] the molar absorption coefficients are larger, which indicates the potential possibility of lowering the practical laser power requirements. As predicted by the computations (Figure 1), the introduction of new branches to the core indeed red-shifted the UV−Vis light absorption profiles of the photoinitiators. Moreover, the trend of the experimental shift in the absorption profile with respect to chemical functionality peak-shifting ability matches the computational results, indicating that the TD-DFT calculations shown are a useful predictive tool for photoinitiator design. Variations in the exact values of experimental measurements and computational results can be attributed to the fact that the TD-DFT calculations assume a vacuum environment for the molecule, whereas the molecules are in solvent during the actual experimental measurement.

In the two most extreme examples (i.e., on the low end and high end of shifts toward the red), the maximum in the absorption peaks for ITX-pyridine and ITX-thiophene are red-shifted relative to ITX by 6 and 17 nm, respectively, and all of the peak absorption values are approaching the target wavelength of 400 nm. Although the extinction coefficients of new photoinitiators are smaller than that of ITX at their respective peaks, most of the extinction coefficients of the new photoinitiators are larger than ITX at 400 nm, highlighting the effectiveness of the design strategy implemented here. The polymerization inhibition process for ITX is controlled by triplet−triplet absorption instead of stimulated emission depletion,[50] which can be represented by fluorescence quantum yield. The photoinitiators synthesized here emit in the range of λ = 414 nm to λ = 431 nm (Figure S8b); however, they have weak fluorescence emission signals, which are similar to those observed for ITX. This indicates that any potential polymerization inhibition is likely to be predominantly from triplet−triplet absorption in this case as well.[50−52]

Besides the first singlet state, the first triplet states (T_1) are essential to understanding the excited state mechanisms as well. Toward this end, phosphorescence spectra at 77 K were obtained.[53] Improved photoinitiator candidates for the 2PP-DLW process were found among the new molecules, which demonstrate longer triplet state lifetimes. As shown in Figures 2 and S9, all the initiators possess clear phosphorescent signals, which illustrates that the transition from the singlet excited state to the triplet state through intersystem crossing exists in all the molecular systems evaluated here. The trend of the phosphorescent lifetimes is listed in Table 1, which represents the sequence of how long each molecule would have their T_1 states populated. As a reference, ITX-Br was also tested, and it had a relatively short phosphorescence lifetime of 38 ms. For most of the new initiator candidates, the phosphorescence lifetimes were moderately increased compared to ITX. The synthesized photoinitiators provide a broad T_1 lifetime range through the varied functional groups attached to the ITX core. The existence of the lengthy triplet states makes the possibility of undergoing the proposed triplet−triplet absorption inhibition mechanism more likely.

Table 1. Single-Photon Absorption Coefficients and Phosphorescent Lifetimes of the Initiators

photoinitiator	λ_{max} (nm)[a]	ε (10^3 mol^{-1} L cm^{-1})[b]	ε (10^3 mol^{-1} L cm^{-1})[c]	λ_{ex} (nm)[d]	λ_{em} (nm)[e]	τ (ms)[f]
ITX	385	7.0	1.6	350	420	120
ITX-pyridine	391	4.6	2.8	365	414	125
ITX-phenyl-CN	393	1.8	1.2	365	414	256
ITX-phenyl	394	4.5	3.7	370	418	148
ITX-phenyl-F	396	5.7	4.8	365	417	144
ITX-phenyl-OCH_3	398	4.2	4.0	365	428	153
ITX-thiophene	402	0.3	0.3	365	431	87

[a]Peak absorption wavelength near 400 nm if there are multiple peaks or shoulders in the spectra. [b]Molar absorption coefficient of the molecules at the wavelength of the peak. [c]Molar absorption coefficient at the 400 nm wavelength. [d]Exciting wavelength used to obtain clear fluorescence and phosphorescence data. [e]Peak fluorescence wavelength of the emission spectrum at room temperature. [f]Phosphorescence lifetime of the molecules at 77 K in toluene.

https://dx.doi.org/10.1021/acsapm.0c01291
ACS Appl. Polym. Mater. XXXX, XXX, XXX−XXX

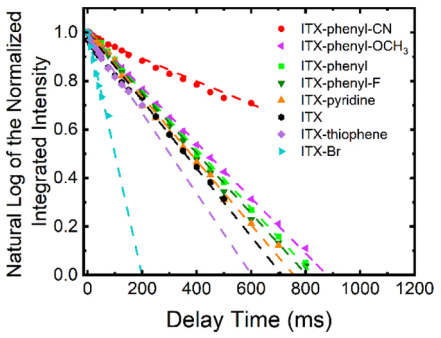

Figure 2. Natural log of the normalized integrated intensity vs delay time spectra of the photoinitiators in toluene at T = 77 K. The slope of each line represents the phosphorescence lifetime, and the spectra shown are ITX-phenyl-CN with a lifetime of 256 ms; ITX-phenyl-OCH_3 with a lifetime of 153 ms; ITX-phenyl with a lifetime of 148 ms; ITX-phenyl-F with a lifetime of 144 ms; ITX-pyridine with a lifetime of 125 ms; ITX with a lifetime of 120 ms; ITX-thiophene with a lifetime of 87 ms; and ITX-Br with a lifetime of 38 ms.

The two-photon cross sections, σ_2, were determined for each molecule by open aperture Z-scan measurements with all the synthesized photoinitiators possessing larger σ_2 values than ITX, which is expected.[54] The two-photon cross-section value is a more promising indicator of improved two-photon absorption during 2PP-DLW compared with one-photon molar absorption. For instance, ITX-thiophene performed notably poorer in terms of molar absorption, but its σ_2 is as strong as those of other candidates. The measured σ_2 values are presented in Figure 3a. To account for unknown experimental setup variables in the Z-scan measurement (e.g., the beam quality), the data were scaled by a constant factor[55] using ITX as calibration from the previous literature.[56] This provides a more accurate representation of the two-photon cross sections for the new photoinitiators relative to one another and ITX. Representative raw data plots that result from the performed Z-scan measurements are shown in Figure S10. Clearly, ITX-thiophene and ITX-OCH_3, both having electron-donating groups, show the largest two-photon cross section. This agrees with the previous observation of molecules that follow a donor−acceptor structure.[31] The molecules with electron-withdrawing groups had smaller cross sections. ITX-pyridine was the least improved. Although all the two-photon cross sections indicate improved absorption by the newly synthesized photoinitiators, efficient two-photon absorption does not directly indicate the polymerization initiation performance.

Therefore, determining the efficiency of these photoinitiators for initiating polymerization is studied by direct application in the DLW polymerization process. For the DLW polymerization testing of the photoinitiators, nanoscale lines of the polymerized materials were printed at 100 μm s^{-1} using separate photoresists containing each initiator. Using a constant print speed ensures equal exposure time across each photoresist. To provide a more direct comparison between all the initiators, each sample consisted of the photoinitiator mixed in the monomer pentaerythritol triacrylate (PETA) at a molar ratio of 0.0025:1 photoinitiator-to-PETA loading. At this molar ratio, all photoinitiators dissolved completely into the monomer (Figure S11), and no solid particles were observed in the resin with a 100 (N.A. = 1.49) magnification microscope. The writing threshold of each photoresist was determined by varying the power of the printing laser. The minimum laser power required to print lines that survived the development process was considered as the writing threshold. A lower writing threshold laser power indicates a more efficient initiator for the DLW process. The writing threshold determined for each photoinitiator mixture is displayed in Figure 3b. Clearly, the synthesized photoinitiators show improved photoinitiating abilities compared to the standard ITX, with ITX-phenyl-OCH_3 showing the most improvement, requiring only 55% of the laser power required for printing with commercial photoinitiator ITX. The trend of the writing thresholds does not entirely follow the trend of two-photon cross sections for the photoinitiators. This has been observed previously,[57] and it is likely due to other processes that participate in efficient photoinitiation of polymerization beyond just the photoabsorption process (e.g., differences in rates of the radical moiety initiating the polymerization of the PETA chains), as has been recently outlined.[21,58,59] Additionally, it can be pointed out that the two-photon cross-section measurements were performed in a different solvent than the DLW. Two-photon absorbing molecules have shown non-

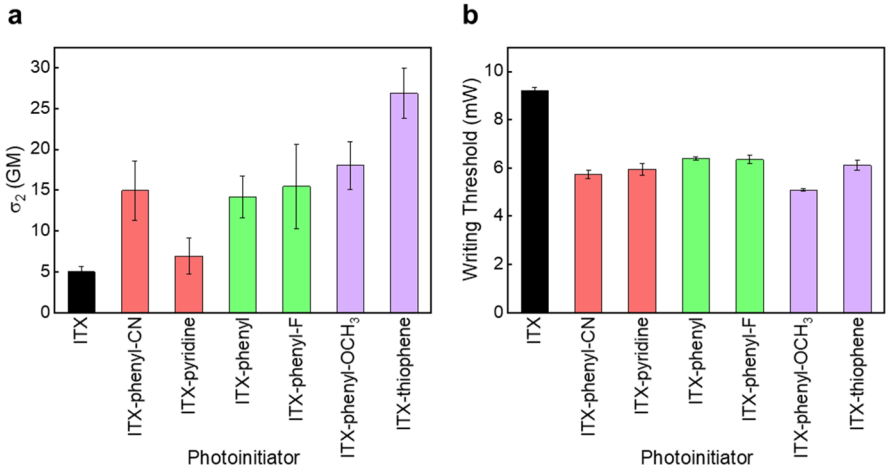

Figure 3. (a) Average two-photon absorption cross-section measurements for photoinitiators measured via the open-aperture Z-scan technique. Three measurements were taken for each photoinitiator. (b) Average writing thresholds for all photoinitiators determined at a 100 μm s^{-1} writing speed and concentration of 0.0025 M ratio of the photoinitiator in the monomer. Thresholds were determined for three different samples of each photoinitiator. All error bars indicate one standard deviation from the average value represented by the bars in the plot.

https://dx.doi.org/10.1021/acsapm.0c01291
ACS Appl. Polym. Mater. XXXX, XXX, XXX−XXX

monotonic solvent dependence, which could be a contributing factor in the observed difference in performance between the two measurements.[60−62]

In addition to testing the DLW ability of the photoresists, the efficiency of inhibiting the polymerization process was evaluated by exposing the resist to varying inhibition laser powers and determining the new writing threshold. In this case, a greater increase in writing threshold under the inhibition laser exposure represented a higher efficiency of the inhibition. This is significant as a photoinitiator with a high inhibition efficiency would require less inhibition laser power, thereby reducing undesired side effects such as heat accumulation. Figure 4 displays the results of the test, where

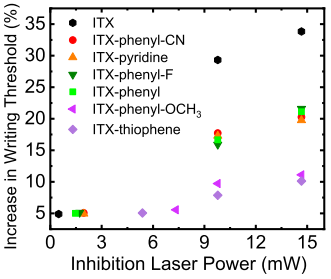

Figure 4. Increase in writing threshold of photoresists consisting of novel and reference photoinitiators while under the exposure of 638 nm inhibition laser at varying powers.

all photoinitiators demonstrated the ability to inhibit polymerization under exposure to a 638 nm laser. The 638 nm laser wavelength was chosen for its similarity to the triplet absorption peak of ITX.[50] Therefore, an efficient inhibition process was expected for ITX, and this was observed in practice. To determine a minimum 638 nm laser power required for inhibiting the polymerization, the writing laser power was set to 5% above the respective writing threshold for each photoinitiator and the inhibiting laser power was systematically varied (Figure 4). The ITX derivatives designed here displayed a less significant inhibition effect because of a shift in the triplet absorption peak in the modified ITX photoinitiators. Indeed, this is supported by TD-DFT calculations, which predict a significant redshift of the triplet absorption peak of the novel photoinitiators compared to ITX (Figure S12). Those molecules following the electron-donating scheme, ITX-phenyl-OCH_3 and ITX-thiophene, exhibit the least impressive inhibition capabilities, which follows from their expected poor triplet absorption at the 638 nm inhibition wavelength owing to the predicted absorption peaks being significantly red-shifted.

Figure 5 shows a representative application of one of the new photoinitiators, ITX-phenyl-OCH_3, at a 0.0025 mol ratio in PETA for 2PP-DLW. Here, several polymer lines were written at 100 μm s^{-1} with a laser power 7% above the writing threshold. For a 10 μm section of the line printing, the 638 nm laser was turned on with 9.8 mW power. The foci of both beams were well overlapped, with the 638 nm laser spot much larger than the printing laser spot. No polymerization was observed in the specified region, indicating complete inhibition of the photoinitiation process. Similar experiments for all other photoinitiators are shown in Figure S13. The width of printed lines varied from ∼100 nm to ∼150 nm for all photoinitiator systems, with lines getting wider for larger writing powers.

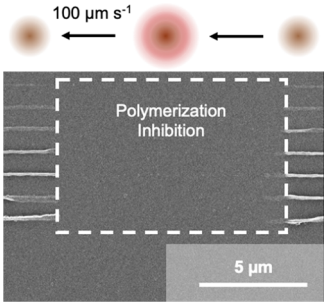

Figure 5. Scanning electron micrograph of polymer lines printed at 100 μm s^{-1} using ITX-phenyl-OCH_3 as a photoinitiator, demonstrating complete inhibition of polymerization under exposure to 638 nm laser (dashed box). The brown spot indicates that the 800 nm printing laser is on, and the red spot indicates that the 638 nm laser is on. The arrows indicate direction of printing. Line height is intentionally varied from top to bottom in steps of 100 nm to ensure that lines are attached to the substrate.

This is a clear demonstration of the ability to control the photopolymerization process of the ITX-phenyl-OCH_3 photoinitiator via a secondary light source. These promising lithography results represent a new photoinitiator set tending toward a superresolution capable photoresist system with reduced printing power requirements, which is ideal for high throughput 3D 2PP-DLW.

CONCLUSIONS

A set of six molecules based on an ITX core was designed and synthesized for use in 2PP-DLW photoinitiator applications. While a desired redshift in absorption was observed for all molecules, those molecules with electron-donating groups exhibited the largest shift toward the target 400 nm absorption wavelength for 2PP-DLW. Indeed, those molecules with electron-donating groups had the most significant absorption improvement at the 2PP-DLW wavelength of 800 nm by Z-scan measurements. Similarly, in DLW experiments, the ITX-phenyl-OCH_3 molecule showed an almost twofold reduction in the writing threshold opposed to the base ITX photoinitiator. In fact, all the newly synthesized photoinitiators presented had significantly improved writing thresholds compared to the ITX molecule. In addition, these molecules are stable and soluble in the photoresist monomer, in contrast to past ITX photoinitiator derivatives. An investigation into the polymerization inhibition properties of the novel photoinitiators yielded an existing polymerization inhibition pathway similar to ITX, though not as efficient at the wavelength evaluated in this study. A further investigation into longer inhibition laser wavelengths may yield significant improvements in the polymerization inhibition efficiency, particularly for the electron-donating molecules. However, the potential for super-resolution nanolithography is clear for these molecules already. In summary, the ITX-derivative photoinitiators presented here are a promising option for more efficient 2PP-DLW, a necessary requirement for increasing nanoprinting throughput through parallelization or similar processes, and an expansion of the currently limited pool of photoinitiators for super-resolution lithography.

https://dx.doi.org/10.1021/acsapm.0c01291
ACS Appl. Polym. Mater. XXXX, XXX, XXX−XXX

■ ASSOCIATED CONTENT

Supporting Information

The Supporting Information is available free of charge at https://pubs.acs.org/doi/10.1021/acsapm.0c01291.

Z-scan measurements concentration table, ^{1}H and ^{13}C NMR spectra, molecular orbital diagrams of initiators, UV−vis absorption and fluorescence spectra, phosphorescence spectra, open-aperture *Z*-scan data and fitting profiles, top and side views of photoresist mixtures, minimum inhibition laser power diagrams, and SEM images of DLW for initiators (PDF)

■ AUTHOR INFORMATION

Corresponding Author

Bryan W. Boudouris − *Department of Chemistry and Charles D. Davidson School of Chemical Engineering, Purdue University, West Lafayette, Indiana 47907, United States;* orcid.org/0000-0003-0428-631X; Email: boudouris@purdue.edu

Authors

Teng Chi − *Department of Chemistry, Purdue University, West Lafayette, Indiana 47907, United States*

Paul Somers − *School of Mechanical Engineering and Birck Nanotechnology Center, Purdue University, West Lafayette, Indiana 47907, United States*

Daniel A. Wilcox − *Charles D. Davidson School of Chemical Engineering, Purdue University, West Lafayette, Indiana 47907, United States*

Ashley J. Schuman − *Department of Chemistry, Purdue University, West Lafayette, Indiana 47907, United States*

Jason E. Johnson − *School of Mechanical Engineering and Birck Nanotechnology Center, Purdue University, West Lafayette, Indiana 47907, United States*

Zihao Liang − *Charles D. Davidson School of Chemical Engineering, Purdue University, West Lafayette, Indiana 47907, United States*

Liang Pan − *School of Mechanical Engineering and Birck Nanotechnology Center, Purdue University, West Lafayette, Indiana 47907, United States*

Xianfan Xu − *School of Mechanical Engineering and Birck Nanotechnology Center, Purdue University, West Lafayette, Indiana 47907, United States;* orcid.org/0000-0003-0580-4625

Complete contact information is available at: https://pubs.acs.org/10.1021/acsapm.0c01291

Author Contributions

T. C. and P. S. contributed equally to this work. T. C. synthesized and measured the linear optical properties of the modified photoinitiators used in this work, as well as assisted in the DFT calculations. P.S. performed the lithographic writing and polymerization inhibition studies of photoinitiators and performed *Z*-scan measurements. D.A.W. performed the DFT calculations. A.S. performed the low-temperature phosphorescence spectroscopy measurements. J.J. determined polymerization thresholds of the photoinitiators and performed polymerization inhibition studies. Z.L. assisted in NMR spectroscopy data collection and data fitting. L.P., X.X., and B.W.B. designed the approach and the experiments associated with the manuscript. All authors contributed to the writing and editing of the manuscript.

Notes

The authors declare no competing financial interest.

■ ACKNOWLEDGMENTS

The majority of the work was supported by the National Science Foundation (NSF) through the Scalable Nanomanufacturing Program (award number: 1634832, Program Manager: Dr. Khershed Cooper), and the work of A.J.S. was also supported by the NSF (award number: 1609151, Program Manager: Dr. George Janini). We thank the NSF for their gracious support. We thank Dr. Aihui Liang from the group of Professor Letian Dou at Purdue University for fruitful discussions.

■ REFERENCES

(1) von Freymann, G.; Ledermann, A.; Thiel, M.; Staude, I.; Essig, S.; Busch, K.; Wegener, M. Three-Dimensional Nanostructures for Photonics. *Adv. Funct. Mater.* **2010**, *20*, 1038−1052.

(2) Frölich, A.; Fischer, J.; Zebrowski, T.; Busch, K.; Wegener, M. Titania Woodpiles with Complete Three-Dimensional Photonic Bandgaps in the Visible. *Adv. Mater.* **2013**, *25*, 3588−3592.

(3) Kaschke, J.; Wegener, M. Gold Triple-Helix Mid-Infrared Metamaterial by STED-Inspired Laser Lithography. *Opt. Lett.* **2015**, *40*, 3986.

(4) Zeng, H.; Wasylczyk, P.; Parmeggiani, C.; Martella, D.; Burresi, M.; Wiersma, D. S. Light-Fueled Microscopic Walkers. *Adv. Mater.* **2015**, *27*, 3883−3887.

(5) Huang, T.-Y.; Sakar, M. S.; Mao, A.; Petruska, A. J.; Qiu, F.; Chen, X.-B.; Kennedy, S.; Mooney, D.; Nelson, B. J. 3D Printed Microtransporters: Compound Micromachines for Spatiotemporally Controlled Delivery of Therapeutic Agents. *Adv. Mater.* **2015**, *27*, 6644−6650.

(6) Martella, D.; Nocentini, S.; Nuzhdin, D.; Parmeggiani, C.; Wiersma, D. S. Photonic Microhand with Autonomous Action. *Adv. Mater.* **2017**, *29*, 1704047.

(7) Xu, B.; Du, W.-Q.; Li, J.-W.; Hu, Y.-L.; Yang, L.; Zhang, C.-C.; Li, G.-Q.; Lao, Z.-X.; Ni, J.-C.; Chu, J.-R.; Wu, D.; Liu, S.-L.; Sugioka, K. High Efficiency Integration of Three-Dimensional Functional Microdevices inside a Microfluidic Chip by Using Femtosecond Laser Multifoci Parallel Microfabrication. *Sci. Rep.* **2016**, *6*, 1−9.

(8) Maruo, S.; Inoue, H. Optically Driven Viscous Micropump Using a Rotating Microdisk. *Appl. Phys. Lett.* **2007**, *91*, 084101.

(9) Alsharhan, A. T.; Acevedo, R.; Warren, R.; Sochol, R. D. 3D Microfluidics via Cyclic Olefin Polymer-Based in Situ Direct Laser Writing. *Lab Chip* **2019**, *19*, 2799−2810.

(10) Frenzel, T.; Kadic, M.; Wegener, M. Three-Dimensional Mechanical Metamaterials with a Twist. *Science* **2017**, *358*, 1072−1074.

(11) Qu, J.; Kadic, M.; Naber, A.; Wegener, M. Micro-Structured Two-Component 3D Metamaterials with Negative Thermal-Expansion Coefficient from Positive Constituents. *Sci. Rep.* **2017**, *7*, 40643.

(12) Bückmann, T.; Stenger, N.; Kadic, M.; Kaschke, J.; Frölich, A.; Kennerknecht, T.; Eberl, C.; Thiel, M.; Wegener, M. Tailored 3D Mechanical Metamaterials Made by Dip-in Direct-Laser-Writing Optical Lithography. *Adv. Mater.* **2012**, *24*, 2710−2714.

(13) Thiele, S.; Arzenbacher, K.; Gissibl, T.; Giessen, H.; Herkommer, A. M. 3D-Printed Eagle Eye: Compound Microlens System for Foveated Imaging. *Sci. Adv.* **2017**, *3*, No. e1602655.

(14) Mayer, F.; Richter, S.; Westhauser, J.; Blasco, E.; Barner-Kowollik, C.; Wegener, M. Multimaterial 3D Laser Microprinting Using an Integrated Microfluidic System. *Sci. Adv.* **2019**, *5*, No. eaau9160.

(15) Mačiulaitis, J.; Deveikytė, M.; Rekštytė, S.; Bratchikov, M.; Darinskas, A.; Šimbelytė, A.; Daunoras, G.; Laurinavičienė, A.; Laurinavičius, A.; Gudas, R.; Malinauskas, M.; Mačiulaitis, R. Preclinical Study of SZ2080 Material 3D Microstructured Scaffolds

for Cartilage Tissue Engineering Made by Femtosecond Direct Laser Writing Lithography. *Biofabrication* **2015**, *7*, 015015.
(16) Zandrini, T.; Shan, O.; Parodi, V.; Cerullo, G.; Raimondi, M. T.; Osellame, R. Multi-Foci Laser Microfabrication of 3D Polymeric Scaffolds for Stem Cell Expansion in Regenerative Medicine. *Sci. Rep.* **2019**, *9*, 11761.
(17) Ovsianikov, A.; Chichkov, B.; Adunka, O.; Pillsbury, H.; Doraiswamy, A.; Narayan, R. J. Rapid Prototyping of Ossicular Replacement Prostheses. *Appl. Surf. Sci.* **2007**, *253*, 6603−6607.
(18) Li, Z.; Hu, P.; Zhu, J.; Gao, Y.; Xiong, X.; Liu, R. Conjugated Carbazole-Based Schiff Bases as Photoinitiators: From Facile Synthesis to Efficient Two-Photon Polymerization. *J. Polym. Sci., Part A: Polym. Chem.* **2018**, *56*, 2692−2700.
(19) Arnoux, C.; Konishi, T.; Van Elslande, E.; Poutougnigni, E.-A.; Mulatier, J.-C.; Khrouz, L.; Bucher, C.; Dumont, E.; Kamada, K.; Andraud, C.; Baldeck, P.; Banyasz, A.; Monnereau, C. Polymerization Photoinitiators with Near-Resonance Enhanced Two-Photon Absorption Cross-Section: Toward High-Resolution Photoresist with Improved Sensitivity. *Macromolecules* **2020**, *53*, 9264−9278.
(20) Kiefer, P.; Hahn, V.; Nardi, M.; Yang, L.; Blasco, E.; Barner-Kowollik, C.; Wegener, M. Sensitive Photoresists for Rapid Multiphoton 3D Laser Micro- and Nanoprinting. *Adv. Opt. Mater.* **2020**, *8*, 2000895.
(21) Fischer, J.; Wegener, M. Three-Dimensional Optical Laser Lithography beyond the Diffraction Limit. *Laser Photonics Rev.* **2013**, *7*, 22−44.
(22) Wollhofen, R.; Katzmann, J.; Hrelescu, C.; Jacak, J.; Klar, T. A. 120 Nm Resolution and 55 Nm Structure Size in STED-Lithography. *Opt. Express* **2013**, *21*, 10831−10840.
(23) Lauer, A.; Fast, D. E.; Kelterer, A.-M.; Frick, E.; Neshchadin, D.; Voll, D.; Gescheidt, G.; Barner-Kowollik, C. Systematic Assessment of the Photochemical Stability of Photoinitiator-Derived Macromolecular Chain Termini. *Macromolecules* **2015**, *48*, 8451−8460.
(24) Ding, G.; Jing, C.; Qin, X.; Gong, Y.; Zhang, X.; Zhang, S.; Luo, Z.; Li, H.; Gao, F. Conjugated Dyes Carrying N, N-Dialkylamino and Ketone Groups: One-Component Visible Light Norrish Type II Photoinitiators. *Dyes Pigm.* **2017**, *137*, 456−467.
(25) Elliott, L. D.; Kayal, S.; George, M. W.; Booker-Milburn, K. Rational Design of Triplet Sensitizers for the Transfer of Excited State Photochemistry from UV to Visible. *J. Am. Chem. Soc.* **2020**, *142*, 14947−14956.
(26) Zivic, N.; Sadaba, N.; Almandoz, N.; Ruipérez, F.; Mecerreyes, D.; Sardon, H. Thioxanthone-Based Photobase Generators for the Synthesis of Polyurethanes via the Photopolymerization of Polyols and Polyisocyanates. *Macromolecules* **2020**, *53*, 2069−2076.
(27) Nazir, R.; Balčiūnas, E.; Buczyńska, D.; Bourquard, F.; Kowalska, D.; Gray, D.; Maćkowski, S.; Farsari, M.; Gryko, D. T. Donor−Acceptor Type Thioxanthones: Synthesis, Optical Properties, and Two-Photon Induced Polymerization. *Macromolecules* **2015**, *48*, 2466−2472.
(28) Breloy, L.; Losantos, R.; Sampedro, D.; Marazzi, M.; Malval, J.-P.; Heo, Y.; Akimoto, J.; Ito, Y.; Brezová, V.; Versace, D.-L. Allyl Amino-Thioxanthone Derivatives as Highly Efficient Visible Light H-Donors and Co-Polymerizable Photoinitiators. *Polym. Chem.* **2020**, *11*, 4297−4312.
(29) Eren, T. N.; Graff, B.; Lalevee, J.; Avci, D. Thioxanthone-Functionalized 1,6-Heptadiene as Monomeric Photoinitiator. *Prog. Org. Coat.* **2019**, *128*, 148−156.
(30) Hola, E.; Pilch, M.; Ortyl, J. Thioxanthone Derivatives as a New Class of Organic Photocatalysts for Photopolymerisation Processes and the 3D Printing of Photocurable Resins under Visible Light. *Catalysts* **2020**, *10*, 903.
(31) Cumpston, B. H.; Ananthavel, S. P.; Barlow, S.; Dyer, D. L.; Ehrlich, J. E.; Erskine, L. L.; Heikal, A. A.; Kuebler, S. M.; Lee, I.-Y. S.; McCord-Maughon, D.; Qin, J.; Röckel, H.; Rumi, M.; Wu, X.-L.; Marder, S. R.; Perry, J. W. Two-Photon Polymerization Initiators for Three-Dimensional Optical Data Storage and Microfabrication. *Nature* **1999**, *398*, 51−54.
(32) Chi, T.; Somers, P.; Wilcox, D. A.; Schuman, A. J.; Iyer, V.; Le, R.; Gengler, J.; Ferdinandus, M.; Liebig, C.; Pan, L.; Xu, X.; Boudouris, B. W. Tailored Thioxanthone-Based Photoinitiators for Two-Photon-Controllable Polymerization and Nanolithographic Printing. *J. Polym. Sci., Part B: Polym. Phys.* **2019**, *57*, 1462−1475.
(33) Harke, B.; Bianchini, P.; Brandi, F.; Diaspro, A. Photopolymerization Inhibition Dynamics for Sub-Diffraction Direct Laser Writing Lithography. *ChemPhysChem* **2012**, *13*, 1429−1434.
(34) Thiel, M.; Ott, J.; Radke, A.; Kaschke, J.; Wegener, M. Dip-in Depletion Optical Lithography of Three-Dimensional Chiral Polarizers. *Opt. Lett.* **2013**, *38*, 4252.
(35) Sheik-Bahae, M.; Said, A. A.; Wei, T.-H.; Hagan, D. J.; Van Stryland, E. W. Sensitive Measurement of Optical Nonlinearities Using a Single Beam. *IEEE J. Quantum Electron.* **1990**, *26*, 760−769.
(36) Fischer, J.; von Freymann, G.; Wegener, M. The Materials Challenge in Diffraction-Unlimited Direct-Laser-Writing Optical Lithography. *Adv. Mater.* **2010**, *22*, 3578−3582.
(37) Creating UV/Visible Plots from the Results of Excited States Calculations Gaussian.com. http://gaussian.com/uvvisplot/ (accessed Oct 21, 2020).
(38) Wu, X.; Jin, M.; Malval, J.-P.; Wan, D.; Pu, H. Visible Light-Emitting Diode-Sensitive Thioxanthone Derivatives Used in Versatile Photoinitiating Systems for Photopolymerizations. *J. Polym. Sci., Part A: Polym. Chem.* **2017**, *55*, 4037−4045.
(39) Coleman, M. P.; Boyd, M. K. S-Pixyl Analogues as Photocleavable Protecting Groups for Nucleosides. *J. Org. Chem.* **2002**, *67*, 7641−7648.
(40) Dadashi-Silab, S.; Bildirir, H.; Dawson, R.; Thomas, A.; Yagci, Y. Microporous Thioxanthone Polymers as Heterogeneous Photoinitiators for Visible Light Induced Free Radical and Cationic Polymerizations. *Macromolecules* **2014**, *47*, 4607−4614.
(41) Ding, L.; Zhang, Z.; Li, X.; Su, J. Highly Sensitive Determination of Low-Level Water Content in Organic Solvents Using Novel Solvatochromic Dyes Based on Thioxanthone. *Chem. Commun.* **2013**, *49*, 7319−7321.
(42) Ding, L.; Zou, Q.; Qu, Y.; Su, J. Novel "Turn-on" Fluorescent Chemodosimeters Based on Thioxanthen-9-Thione for the Selective Detection of Mercuric Ions in Aqueous Media. *RSC Adv.* **2012**, *2*, 4754−4758.
(43) Ding, L.; Wu, M.; Li, Y.; Chen, Y.; Su, J. New Fluoro- and Chromogenic Chemosensors for the Dual-Channel Detection of Hg2+ and F−. *Tetrahedron Lett.* **2014**, *55*, 4711−4715.
(44) Orazietti, M.; Kuss-Petermann, M.; Hamm, P.; Wenger, O. S. Light-Driven Electron Accumulation in a Molecular Pentad. *Angew. Chem., Int. Ed.* **2016**, *55*, 9407−9410.
(45) Miyaura, N.; Yamada, K.; Suzuki, A. A New Stereospecific Cross-Coupling by the Palladium-Catalyzed Reaction of 1-Alkenylboranes with 1-Alkenyl or 1-Alkynyl Halides. *Tetrahedron Lett.* **1979**, *20*, 3437−3440.
(46) Miyaura, N.; Suzuki, A. Stereoselective Synthesis of Arylated (E)-Alkenes by the Reaction of Alk-1-Enylboranes with Aryl Halides in the Presence of Palladium Catalyst. *J. Chem. Soc., Chem. Commun.* **1979**, *19*, 866−867.
(47) Miyaura, N.; Suzuki, A. Palladium-Catalyzed Cross-Coupling Reactions of Organoboron Compounds. *Chem. Rev.* **1995**, *95*, 2457−2483.
(48) Dahlstedt, E.; Collins, H. A.; Balaz, M.; Kuimova, M. K.; Khurana, M.; Wilson, B. C.; Phillips, D.; Anderson, H. L. One-and Two-Photon Activated Phototoxicity of Conjugated Porphyrin Dimers with High Two-Photon Absorption Cross Sections. *Org. Biomol. Chem.* **2009**, *7*, 897−904.
(49) Albota, M.; Beljonne, D.; Brédas, J.-L.; Ehrlich, J. E.; Fu, J.-Y.; Heikal, A. A.; Hess, S. E.; Kogej, T.; Levin, M. D.; Marder, S. R.; McCord-Maughon, D.; Perry, J. W.; Röckel, H.; Rumi, M.; Subramaniam, G.; Webb, W. W.; Wu, X.-L.; Xu, C. Design of Organic Molecules with Large Two-Photon Absorption Cross Sections. *Science* **1998**, *281*, 1653−1656.
(50) Harke, B.; Dallari, W.; Grancini, G.; Fazzi, D.; Brandi, F.; Petrozza, A.; Diaspro, A. Polymerization Inhibition by Triplet State

https://dx.doi.org/10.1021/acsapm.0c01291
ACS Appl. Polym. Mater. XXXX, XXX, XXX−XXX

Absorption for Nanoscale Lithography. *Adv. Mater.* **2013**, *25*, 904−909.
(51) Amirzadeh, G.; Schnabel, W. On the Photoinitiation of Free Radical Polymerization-Laser Flash Photolysis Investigations on Thioxanthone Derivatives. *Die Makromolekulare Chem.* **1981**, *182*, 2821−2835.
(52) Aydin, M.; Arsu, N.; Yagci, Y.; Jockusch, S.; Turro, N. J. J. Mechanistic Study of Photoinitiated Free Radical Polymerization Using Thioxanthone Thioacetic Acid as One-Component Type II Photoinitiator. *Macromolecules* **2005**, *38*, 4133−4138.
(53) Kuboyama, A. The Phosphorescence Spectra of 1,4-Naphthoquinone and Its Alkyl Derivatives in Solutions at 77 K. *Bull. Chem. Soc. Jpn.* **1978**, *51*, 2771−2775.
(54) Chung, S.-J.; Kim, K.-S.; Lin, T.-C.; He, G. S.; Swiatkiewicz, J.; Prasad, P. N. Cooperative Enhancement of Two-Photon Absorption in Multi-Branched Structures. *J. Phys. Chem. B* **1999**, *103*, 10741−10745.
(55) Bridges, R. E.; Fischer, G. L.; Boyd, R. W. Z-Scan Measurement Technique for Non-Gaussian Beams and Arbitrary Sample Thicknesses. *Opt. Lett.* **1995**, *20*, 1821−1823.
(56) Schafer, K. J.; Hales, J. M.; Balu, M.; Belfield, K. D.; Van Stryland, E. W.; Hagan, D. J. Two-Photon Absorption Cross-Sections of Common Photoinitiators. *J. Photochem. Photobiol., A* **2004**, *162*, 497−502.
(57) Whitby, R.; Ben-Tal, Y.; MacMillan, R.; Janssens, S.; Raymond, S.; Clarke, D.; Jin, J.; Kay, A.; Simpson, M. C. Photoinitiators for Two-Photon Polymerisation: Effect of Branching and Viscosity on Polymerisation Thresholds. *RSC Adv.* **2017**, *7*, 13232−13239.
(58) Fast, D. E.; Lauer, A.; Menzel, J. P.; Kelterer, A.-M.; Gescheidt, G.; Barner-Kowollik, C. Wavelength-Dependent Photochemistry of Oxime Ester Photoinitiators. *Macromolecules* **2017**, *50*, 1815−1823.
(59) Frick, E.; Schweigert, C.; Noble, B. B.; Ernst, H. A.; Lauer, A.; Liang, Y.; Voll, D.; Coote, M. L.; Unterreiner, A.-N.; Barner-Kowollik, C. Toward a Quantitative Description of Radical Photoinitiator Structure-Reactivity Correlations. *Macromolecules* **2016**, *49*, 80−89.
(60) Woo, H. Y.; Liu, B.; Kohler, B.; Korystov, D.; Mikhailovsky, A.; Bazan, G. C. Solvent Effects on the Two-Photon Absorption of Distyrylbenzene Chromophores. *J. Am. Chem. Soc.* **2005**, *127*, 14721−14729.
(61) Nag, A.; Goswami, D. Solvent Effect on Two-Photon Absorption and Fluorescence of Rhodamine Dyes. *J. Photochem. Photobiol., A* **2009**, *206*, 188−197.
(62) Tan, Y.; Zhang, Q.; Yu, J.; Zhao, X.; Tian, Y.; Cui, Y.; Hao, X.; Yang, Y.; Qian, G. Solvent Effect on Two-Photon Absorption (TPA) of Three Novel Dyes with Large TPA Cross-Section and Red Emission. *Dyes Pigm.* **2013**, *97*, 58−64.

https://dx.doi.org/10.1021/acsapm.0c01291
ACS Appl. Polym. Mater. XXXX, XXX, XXX−XXX